Common dynamical signatures of familial amyotrophic lateral sclerosis-associated structurally diverse Cu, Zn superoxide dismutase mutants

Sagar D. Khare* and Nikolay V. Dokholyan†

Department of Biochemistry and Biophysics, University of North Carolina School of Medicine, Chapel Hill, NC 27599

Communicated by Aziz Sancar, University of North Carolina School of Medicine, Chapel Hill, NC, December 30, 2005 (received for review November 1, 2005)

More than 100 structurally diverse point mutations leading to aggregation in the dimeric enzyme Cu, Zn superoxide dismutase (SOD1) are implicated in familial amyotrophic lateral sclerosis (FALS). Although SOD1 dimer dissociation is a known requirement for its aggregation, the common structural basis for diverse FALS mutations resulting in aggregation is not fully understood. In molecular dynamics simulations of wild-type SOD1 and three structurally diverse FALS mutants (A4V, G37R, and H46R), we find that a common effect of mutations on SOD1 dimer is the mutation-induced disruption of dynamic coupling between monomers. In the wild-type dimer, the principal coupled motion corresponds to a ''breathing motion'' of the monomers around an axis parallel to the dimer interface, and an opening–closing motion of the distal metal-binding loops. These coupled motions are disrupted in all three mutants independent of the mutation location. Loss of coupled motions in mutant dimers occurs with increased disruption of a key stabilizing structural element (the β-plug) leading to the de-protection of edge strands. To rationalize disruption of coupling, which is independent of the effect of the mutation on global SOD1 stability, we analyze the residue–residue interaction network formed in SOD1. We find that the dimer interface and metal-binding loops, both involved in coupled motions, are regions of high connectivity in the network. Our results suggest that independent of the effect on protein stability, altered protein dynamics, due to long-range communication within its structure, may underlie the aggregation of mutant SOD1 in FALS.

β-plug | A4V | G37R | H46R | protein dynamics

Point mutations in the cytoplasmic homodimeric enzyme Cu, Zn superoxide dismutase (SOD1) (1) have been identified as the primary cause of ≈20% cases of the disease familial amyotrophic lateral sclerosis (FALS) (2, 3). There are >100 distinct and structurally diverse FALS mutations known to result in identical symptoms (4), suggesting that all mutations affect an unknown common property of the protein, leading to toxicity. There is evidence that the motor neuron-specific toxic gain-of-function of the mutants is associated with intracellular aggregation, trafficking, and/or degradation of misfolded SOD1 (5, 6). The inhibition of aggregation by overexpression of chaperones leads to increased cell viability (7).

The molecular mechanism of misfolding and aggregation of SOD1, and how structurally and chemically diverse mutations lead to aggregation, is not fully understood. We and others have previously demonstrated that the *in vitro* aggregation of SOD1 occurs via a pathway involving dissociation of the dimer and loss of metals, followed by multimeric assembly of the apo-monomeric (metal-free) SOD1 (8–10). FALS mutations are likely to lead to enhanced aggregation by affecting one or more steps in the aggregation pathway leading to an increase in the population of the aggregation-prone apo-monomer. Inhibition of mutant SOD1 dimer dissociation by engineering an intersubunit disulfide bond on the interface or by small-molecule binding drastically reduces or abolishes aggregation (9, 11). For a subset of mutants, the decrease in stability of the mutant apo-dimer correlates with the average survival time of patients carrying the mutation, suggesting that stability of the dimer may be a ''common denominator'' underlying FALS (12, 13). However, for other structurally distinct mutants, mutation is found to stabilize the apo-state of the protein, while still causing disease, suggesting that the decreased stability is not sufficient for explaining the enhanced aggregation propensity of mutants (14).

The lack of specificity in mutations coincident with an identical aggregation phenotype indicates the high connectivity of the scattered mutation sites with sites that maintain the fold fidelity of SOD1. It is expected that mutants affect the global dynamics of SOD1 in the native state and lead to greater sampling of aggregation-prone states. Indeed, several mutants are known to be more dynamic: they are more susceptible to the reduction of the conserved disulfide bond in SOD1 (15), display enhanced binding to hydrophobic beads (16), have greater H/D exchange rates (14), and have enhanced mobility in specific regions of the protein on the picosecond–nanosecond time scale, compared with wild-type SOD1 (17). Given the higher flexibility of the mutants, mutant SOD1 may induce aggregation by enhancing the propensity to locally (for both stabilizing and destabilizing mutants) and globally (for destabilizing mutants) unfold, leading to the exposure of aggregation-inducing structural elements. Hence, understanding how structural perturbation associated with different FALS mutations influences the global and local dynamics of SOD1, particularly of the aggregation-prone regions, can provide clues for delineating the common underlying basis of mutation-associated aggregation.

In many cellular processes, energy change associated with perturbations such as mutations or ligand binding is transduced through a protein structure, linking residues within or between subunits (18, 19). This long-range communication within protein structures has been uncovered by using both experimental and theoretical approaches, and these approaches have shown that the free energy change at one site is not transduced uniformly through the protein structure; instead it is directed to specific regions of the protein (20). These regions are determined by the geometry and the connectivity of the structural network of the protein (21).

Here we ask how and why diverse FALS mutations affect the local, near-native dynamics of the apo-SOD1 dimer and monomer, and how the altered dynamics leads to the disruption of fold fidelity in SOD1 that may result in its aggregation. We choose three structurally and thermodynamically diverse mutations (Fig. 5, which is published as supporting information on the PNAS web site): (*i*) A4V, a highly destabilizing mutation on the dimer interface; (*ii*) G37R, a destabilizing mutation in the β-plug region close to the hydrophobic core; and (*iii*) H46R, a mildly stabilizing

Conflict of interest statement: No conflicts declared.

Abbreviations: FALS, familial amyotrophic lateral sclerosis; MD, molecular dynamics; RMSD, root mean square deviation; SOD1, Cu, Zn superoxide dismutase.

*Present address: Department of Biochemistry, University of Washington, Seattle, WA 98195.

†To whom correspondence should be addressed. E-mail: dokh@med.unc.edu.

BIOPHYSICS

mutation in an active-site loop. We find that independent of the affect on global protein stability and the location of mutation, mutant SOD1 displays a loss of coupling between the motions of monomer subunits in the dimer. Furthermore, we find that the hydrogen-bond network stabilizing the putatively aggregation-prone edge strands and the hydrophobic β-plug region (Fig. 5) is also weakened in the mutant dimers and monomers compared with wild type and upon exposure of the wild-type dimer to aggregation-promoting conditions. We rationalize the disruption of intermonomer coupling in mutants by analyzing the connectivity properties of the SOD1 β-barrel fold and find that the topology of the SOD1 fold may underlie the observed (loss of) coupling. Our results suggest that the dynamics of SOD1 helps explain the observed diversity of mutations in SOD1 that lead to its aggregation in FALS.

Results and Discussion

We perform all-atom molecular dynamics (MD) simulations of dimers and monomers of wild-type SOD1 and three mutants for 5 ns each in a box of water (see *Materials and Methods*). To understand the effect of mutation on protein dynamics on the picosecond–nanosecond time scale, we compare dynamical properties, calculated from the simulation trajectories, of the mutants with the wild type, and the dimers with the monomers.

The root mean square deviation (RMSD) of the backbone atoms from the respective minimized crystal structure in the protein is <2.5 Å for all dimers (Fig. 1 *a–d*) and <2 Å for all monomers (Fig. 1 *e–h*). The RMSD of the dimer interface mutant, A4V, monomer has an increasing trend with time, suggesting that a structural rearrangement occurs within this monomer on the nanosecond time scale, and that a significant destabilization of the protein occurs as a result of the addition of hydrophobic groups (Ala to Val) on the water-exposed dimer interface of the monomer. However, with the exception of the A4V monomer, we find that all other trajectories do not show large drifts in RMSD and sample near-native conformations (Fig. 1 *a–h*). Whereas A4V and G37R are known to destabilize SOD1, the H46R mutant is known to stabilize SOD1 (13, 14), and accordingly the MD trajectories of H46R have the minimum RMSD among all trajectories.

Altered Fluctuation Patterns of Residues in Mutant SOD1 Dimers. To understand whether and how mutation affects the dynamics of SOD1 dimer on a picosecond–nanosecond time scale, we calculate the fluctuations of each residue in the wild-type and mutant dimers. We calculate the internal mobility of any given residue, *i*, i.e., fluctuations of the residue relative to the average fluctuation of all residues in the protein (see *Materials and Methods*). The resulting normalized fluctuation of a residue, $Z(i)$, is compared between trajectories by calculating the change in the internal mobility of the residue, $\Delta Z = Z(i, \text{wild type}) - Z(i, \text{mutant})$. We find that mutants have a significantly altered pattern of mobility compared with wild type (Fig. 1 *i–k*). In the A4V, H46R, and G37R mutants, 62%, 53%, and 64% of the residues in the dimer are more flexible than the wild type, respectively, indicating that as a consequence of the altered packing, residues are globally more flexible in the mutants than in the wild-type dimer (Fig. 1 *i–k*). However, there are several residues that are less flexible in the mutants; for example, the residues 70–80 in the zinc loop are more flexible in the wild-type dimer than in the A4V and H46R mutants. On the other hand, the N and C termini and the residues 133–138 in the electrostatic loop, which form a helix, are more flexible in all mutants, compared with the wild type. In good agreement with our calculations, these helix-forming residues 133–144 have also been found to be more flexible (have higher crystallographic *B*-factors) in the G37R mutant crystal structure (22). The altered flexibility of mutant dimers suggests that certain modes of motion occurring in the wild-type dimer are absent in the mutant dimers, and vice versa.

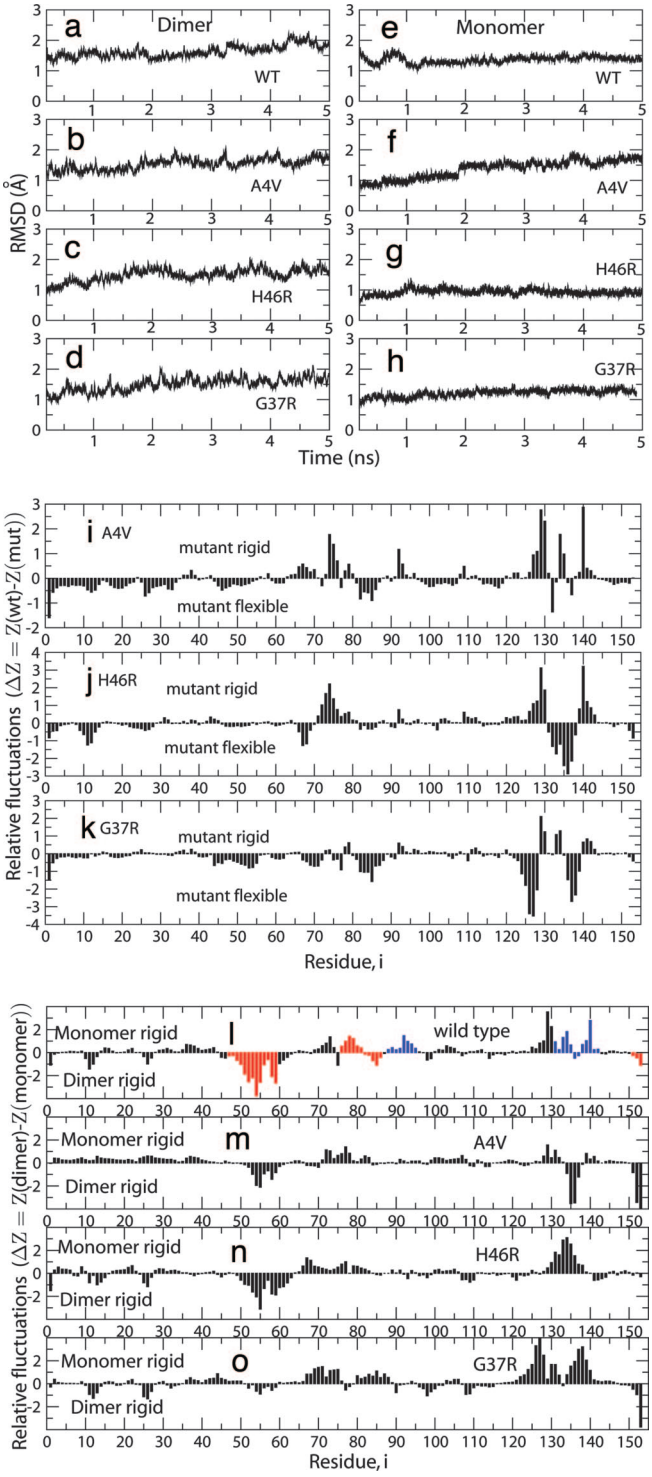

Fig. 1. Flexibility of residues in MD trajectories. (*a–h*) The RMSD of the MD trajectories from the original minimized crystal structure. (*i–k*) Relative fluctuations of residues in the mutant dimers compared with fluctuation in wild-type SOD1. Only one monomer (A in the crystal structure of the wild type) is shown for comparison. (*l–o*) Relative fluctuations of residues in the wild-type and mutant monomers compared with the fluctuation in the respective dimer. In *l*, residues experimentally found to be more/less rigid in the dimer compared with the monomer are colored red/blue, respectively.

Distinct Loss of Intersubunit Coupling in Mutant SOD1 Dimers. Altered patterns of flexibility in the mutants compared with the wild type may arise because of altered packing of the residues in the dimer.

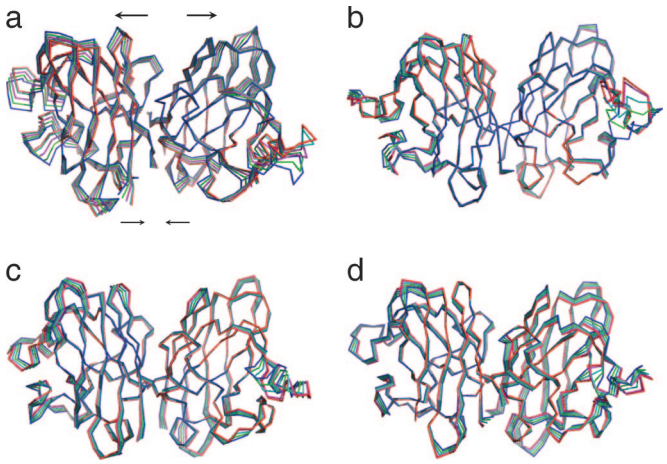

Fig. 2. The first eigenmode obtained from essential dynamics analysis projected on the structures of wild-type (*a*), A4V (*b*), H46R (*c*), and G37R (*d*) dimers. In the wild type, a global breathing motion of the monomers is indicated by arrows.

The packing strain induced by mutation at one site is propagated to other residues in the protein, thus affecting the correlated motions of the residues. To elucidate the motion types that are altered by mutations in SOD1 dimer, for each mutant and wild-type dimer we calculate the interresidue covariance matrix (Eq. **1**), which measures the coupling between the motion of any pair of residues on the picosecond–nanosecond time scale accessed in the simulation (*Materials and Methods*). We find that there are distinctly pronounced patterns of correlation between residues in the wild-type dimer (Fig. 6*a*, which is published as supporting information on the PNAS web site) at 300 K, which are significantly diminished in the three mutant dimers (Fig. 6 *b–d*). These couplings in the wild-type dimer have been observed in previous shorter-time-scale MD studies (23). In all trajectories, secondary elements of the native structure show a high correlation with each other, indicating that all dimers sample near-native states. However, in the wild-type dimer, there are a large number of long-range positively correlated (square III) and, more prominently, anticorrelated motions (square IV), including both intra- and intermonomer motions exhibited by pairs of residues (Fig. 6*a*). Whereas a majority of the positively correlated motions are between residues that are sequence neighbors or are in contact in the native state, a majority of the anticorrelated motions are between residues in the active-site loops (60–80 and 120–140) and other regions of the protein, suggesting an opening–closing motion of the loops. Such motion allows substrate diffusion to the active site of the enzyme. Previous studies of enzyme MD by Bruice and coworkers (24) have also identified anticorrelated motions of the active sites as signatures of enzymatic activity. Thus, correlated motions between monomers arise on the nanosecond time scale and are, remarkably, disrupted in the mutant dimers.

To quantify the degree of decoupling induced by the mutation, we calculate the contribution of intermonomer correlated motions to the overall correlations in the dimer. This contribution is defined as

$$C_{\text{inter}} = \left(\sum_{i,j} c_{ij}^{\text{intra1}} + \sum_{i,j} c_{ij}^{\text{intra2}} + \sum_{i,j} c_{ij}^{\text{inter}} \right)^{-1} \times \sum_{i,j} c_{ij}^{\text{inter}},$$

where c_{ij} is the absolute value of the correlation coefficient between residues i and j, the superscripts "intra1" and "intra2" represent correlations within the two monomers, and "inter" represents correlations between the two monomers. The values of C_{inter}, the fraction of the correlation that is intermonomer, are 0.26, 0.07, 0.12, and 0.14 for the wild-type and A4V, H46R, and G37R mutant dimers, respectively, showing that the coupling between the monomers is considerably reduced in all three mutants compared with the wild type. The values C_{intra1} and C_{intra2}, defined similarly as C_{inter}, also change upon mutation (Table 1, which is published as supporting information on the PNAS web site). We find that the wild type has greater intramonomer correlations than the mutants, indicating that strain introduced by the mutation disrupts not only intermonomer motions, but also intramonomer concerted motions of secondary structural elements.

Altered correlation patterns between residue pairs in the mutants suggest that the major global dynamic modes of the protein involving motions of secondary and tertiary structures are altered upon mutation. To elucidate these global dominant motions in the wild type that lead to the observed coupling and that are disrupted in the mutants, we use the essential dynamics method (25), which is based on projecting the correlated fluctuations in the protein to a principal-components "essential" subspace (*Materials and Methods*). The eigenvectors and eigenvalues of the covariance matrix represent the directions and amplitudes of motions in the principal components subspace (Fig. 2). We find that for the wild type and A4V, H46R, and G37R mutants, the first 5–10 modes, arranged in decreasing order of their eigenvalues, capture a majority ($\approx$75%) of the protein motions (Fig. 7, which is published as supporting information on the PNAS web site). We find pronounced differences in the first, most dominant, eigenmode between the wild-type and the mutant dimers (Fig. 2).

In the first eigenmode, the wild-type dimer exhibits a "breathing" motion around an axis parallel to the dimer interface, along with an opening–closing motion of its loops. This motion, which is global and is a coupled motion between the two dimers, is absent in all of the mutants. Instead, the dominant motion modes of mutant dimers are confined to the active sites and, in some cases, other loops of the protein. Importantly, the loss of global coupling in the mutants occurs irrespective of the location of the mutation: the A4V mutation is on the dimer interface, the G37R is in the β-plug region, and the H46R is in the metal-binding site. Also, the lack of coupling is independent of the effect of mutation on stability; A4V and G37R are known to destabilize the protein, whereas H46R is known to stabilize apo-SOD1.

We postulate that breathing motions provide a mechanism for the dissipation of energy perturbations induced by the environment. In the mutants, because of the evident absence of this breathing global mode on the picosecond–nanosecond time scale, the energy perturbation may instead cause the local unfolding of key structural features of the protein and may thus enhance aggregation propensity, independent of the effect of mutation on the global protein stability.

Dynamical Effects of Dimer Dissociation. Dimer dissociation is known to be required for the aggregation of SOD1 (8), and SOD1 folding is known to be a three-state process involving the folding of individual monomers followed by their association (26). The crystal structure of a monomeric mutant of SOD1 shows that the isolated monomers maintain the canonical eight-stranded Greek key barrel fold of the SOD1 dimer (27). Because monomers are on-pathway to aggregation, changes in the flexibility of monomer substructures upon dimer dissociation likely provide structural clues to the propensities of specific areas of the monomer to induce aggregation.

To probe the dynamical effects of dimer dissociation on SOD1, we perform 5-ns-long MD simulations of the wild-type and three mutant SOD1 monomers, and compare monomer dynamics to that of the corresponding dimer on an identical time scale. We find that all monomer trajectories, except for the A4V monomer, which has an increasing trend in RMSD (Fig. 1*f*), display lower or similar RMSD compared with the dimers, suggesting that isolated monomers are stable on the picosecond–nanosecond time scale. We

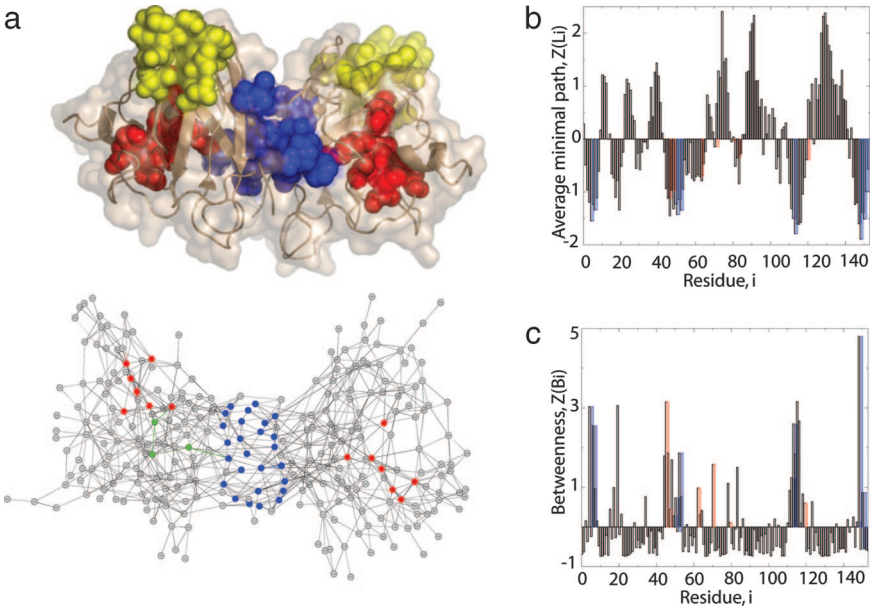

Fig. 3. The network of interactions in SOD1. (*a*) A representation of the graph of the SOD1 dimer. Each node corresponds to a residue, and an edge exists between the nodes if they form a van der Waals contact. The dimer interface residues are colored blue, and the residues in the metal-binding sites are colored red. An example minimal path from L8 to the dimer interface and to the metal-binding sites is shown in green. The β-plug residues are colored yellow. (*b* and *c*) The distribution of normalized average minimal paths from a given residue to all other residues in the protein (*b*) and the betweenness of each residue (*c*).

calculate the changes upon dimer dissociation in the flexibility of each residue relative to the rest of the protein (Fig. 1 *l–o*). We find that in wild-type SOD1, residues 9–13, 25–27, 38–62, 82–86, and 151–153 are more rigid in the dimer, whereas residues 37–43, 70–80, 88–95, and 125–142 are more rigid in the monomer. These findings are in good agreement with NMR experiments of Banci *et al.* (28), in which they find that 47–59, 76–86, and 151–153 are more rigid in the dimer, whereas residues 131–142 and 88–95 are more rigid in the monomer. The measurements of NMR order parameters by Banci *et al.* were performed for holo-dimer, whereas our simulations, although starting with the holo-protein structure for the wild type, are performed on the apo-dimer. In a crystal structure of SOD1 wild-type native dimers that are 80% metal deficient, relatively minor structural rearrangements occur compared with the fully metallated protein without changes in the overall SOD1 fold (29). The prominent effect of metals is on the overall thermodynamic stability of the protein, which is considerably reduced by the loss of metals, and leads to an enhanced propensity to unfold. The unfolding of SOD1 dimer occurs on the millisecond–second time scale (13), whereas our simulations and NMR order parameters both sample the picosecond–nanosecond time scale. Therefore, the observed agreement of residue flexibilities in apo-SOD1 (our simulations) and holo-SOD1 (NMR experiments) dimers and monomers indicates that dynamical properties of the holo- and the apo-forms of SOD1 on the picosecond–nanosecond time scale may be similar.

The differences in the rigidities of dimer and monomers follow similar trends in the stabilizing H46R mutant as the wild type but follow a different pattern in the A4V and G37R mutants. In A4V, the residues 134–138, part of the active site loop, are found to be more flexible in the monomer than in the dimer, and the increasing RMSD of the A4V with time can be attributed to the greater disorder in the Zn-loop. The Zn-loop is known to be a site of nonnative contacts in a crystal structure of multimeric SOD1 assemblies (30). In G37R, the residues 48–62, which form a loop at the dimer interface (residues 50–53 make intermonomer contacts), are found to be less flexible upon dimer dissociation compared with wild type and other mutants. However, in all mutants, the region 88–95, which forms a loop at the edge strand of SOD1 and is part of the stabilizing "β-plug" group of residues, is nearly equally flexible in the mutant dimers compared with monomers (Fig. 1 *m–o*), in contrast with the wild-type protein (Fig. 1*l*), where it is found to rigidify upon dimer dissociation.

Mutation- and Dissociation-Induced Changes in the Conformational Stability of the β-Plug. The group of residues 37–43, 90–92, 94, and 144 comprise the β-plug region of the SOD1 dimer (22). The residues 90–95 are part of the loop connecting strands β5 and β6 in SOD1, which is the site of a putative edge strand of the β-barrel, where the cylindrical hydrogen bonding patterns, which maintain the barrel geometry, are disrupted. Richardson and Richardson (31) have suggested that edge strands are likely sites for aggregation in proteins. Therefore, we evaluate the effect of three aggregation-promoting conditions (mutation, dimer dissociation, and exposure to high temperature) on the dynamics of the loop formed by residues 90–95. To evaluate the effect of exposure to high temperature, we perform 5-ns MD simulations of wild-type SOD1 at 400 K (Fig. 8, which is published as supporting information on the PNAS web site).

We find that the mutant SOD1 dimers exhibit altered dynamics in the 90–95 loop. The altered dynamics is concomitant with the loss of stabilizing hydrogen bonds within the loop and with other residues of the β-plug region 37–43 (Table 2, which is published as supporting information on the PNAS web site). An examination of the first dominant eigenmode of the wild-type dimer, wild-type monomer, and three mutant dimers indicates that in the wild-type dimer these loop-forming residues undergo a twisting motion so that β5 and β6 strands they connect maintain their hydrogen bonds with the β-plug of the SOD1 barrel (Fig. 9*a*, which is published as supporting information on the PNAS web site). On the other hand, in the monomer, in the mutant dimers and in the wild-type dimer at 400 K, residues 90–95 are rigidified, so that the β-plug is destabilized by the loss of hydrogen bonds and the β5 and β6 strands exhibit a tendency to move away from each other, resulting in a transient opening of the SOD1 β-barrel (Fig. 9 *b* and *c*). The dihedral angles of the backbone populated by residues 91–94 during the trajectories further reinforce the rigidification of the loop under destabilizing conditions (Fig. 9). Residues 91–93 in the dimer undergo transitions between dihedral angles only in the wild type, but not upon mutation, dimer dissociation, or, remarkably, at 400 K. Instead, the strain in the loop is transmitted to the β5 and β6 strands, which show increased propensity to move in opposite directions. Therefore, we conclude that mutation, dimer dissociation, and exposure to mildly destabilizing conditions, all known to promote aggregation, promote the disruption of the structural fidelity of the β-plug and result in an increased propensity of the SOD1 β-barrel to transiently open.

The destabilization of the β-plug was previously observed in the crystal structure of the G37R mutant (22). Similarly, in an NMR study of the G93A mutant SOD1 dimer, it was found that the edge-strands had higher mobility compared with wild type (17). However, both residues 37 and 93 are part of the plug region, so it was not clear whether the β-plug destabilization is a general mechanism or is limited to these mutants. Our results indicate that mutations in residues distal from the β-plug (such as residues 4 and 46) may also dynamically destabilize it, even though they have differing effects on the global stability of SOD1, leading to a transient opening of the β-barrel (see Tables 1 and 2). A prediction from our study, which can be tested in NMR experiments, is that the native state dynamics of the A4V and H46R is affected to induce higher disorder in of the β-plug region compared with wild type.

Rationalizing the Loss of Intersubunit Coupling in Mutants. To rationalize the observed loss of coupling between monomers in the mutants, we analyze the network of interactions formed in the structure of native SOD1 dimer and monomers (Fig. 3*a*) and characterize the distribution of minimal path lengths, L_{ij}, from residue i to the residue j (see *Materials and Methods*). For each residue i, we calculate the average minimal path, a measure of the connectivity of the residue to the rest of the network, to all other residues, $\langle L_i \rangle$, to the dimer interface $\langle L_{iI} \rangle$, and to the metal-binding site $\langle L_{iM} \rangle$, by averaging over the minimal paths to all other residues in the protein, to residues on the dimer interface and in the metal-binding site, respectively (Fig. 10, which is published as supporting information on the PNAS web site). For the dimer, we consider the corresponding residues from both monomers as comprising the respective sites.

The value $\langle L_i \rangle$ is an indicator of the global connectivity of residue i: a small $\langle L_i \rangle$ value [corresponding to a negative value of $Z(\langle L_i \rangle)$] indicates that any perturbation, such as a mutation, at the residue i will be transmitted effectively to all other residues in the protein. For the dimer, we find that there are five regions that have high connectivity to the rest of the protein (Fig. 3*b*): residues 2–9, 16–21, 43–65, 109–119, and 144–153. All of the residues on the dimer interface lie in the identified regions of high connectivity. Surprisingly, of the residues chelating the metals, residues 46, 48, and 63 are highly connected, even though these are not in the protein core, and away from the dimer interface. Similar results are obtained for the betweenness B_i profile (Fig. 3*c*). Residues with high betweenness are the hubs in the network through which a large number of paths linking various pairs of residues pass. These observations indicate that both the dimer interface and the metal-binding sites in the dimer are highly connected to the rest of the protein, and mutations in these residues would likely lead to a global protein destabilization. Conversely, a perturbation at any protein site due to mutation is likely to affect both the dimer interface and metal coordinating sites through the network of contact interactions and may disrupt their coupled motions.

To probe whether the effect of a mutation on the dimer interface is correlated with its effect on the metal-coordinating sites, we calculate the average minimal path of all residues to the dimer interface and metal coordinating residues (Fig. 10*a*). We find that, for each residue, these distances, $\langle L_{iI} \rangle$ and $\langle L_{iM} \rangle$, are highly correlated to each other in the dimer (Pearson correlation coefficient $r^2 \approx 0.8$), but neither $\langle L_{iI} \rangle$ nor $\langle L_{iM} \rangle$ correlate with the distance of the residue to another region of the protein (chosen as control); the correlation is also absent in the monomer (Fig. 10), showing that the correlation between the minimal paths to the dimer interface and the metal-binding site in the dimer is specific and significant. Thus, a perturbation such as mutation at any site in the protein is likely to affect simultaneously the dimer interface and the metal sites. We postulate that this connectivity rationalizes the disruption of the coupling between the two monomers, because the coupled elements, the interface and the metal-binding loops, are both likely perturbed by the mutation.

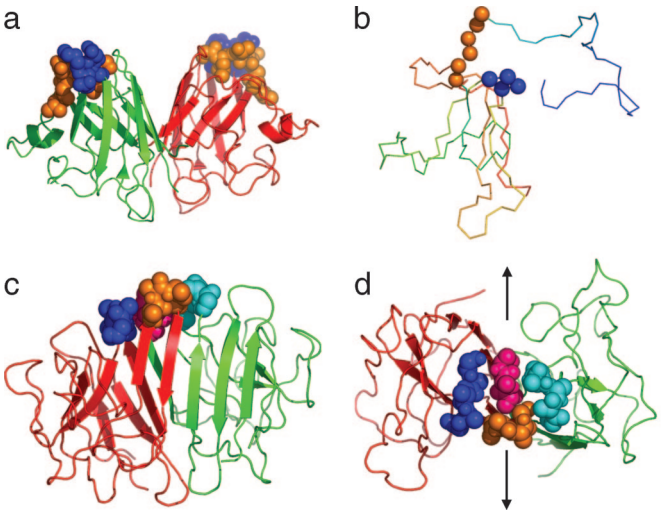

Fig. 4. A model for the aggregation of SOD1 involving the β-plug region. (*a*) The native SOD1 dimer. The residues 37–42 and 90–95 comprising the β-plug are colored in orange and blue, respectively. (*b*) An intermediate misfolded monomer observed in previous MD simulations of model SOD1 monomer unfolding (32) involving a disrupted β-plug region. (*c* and *d*) Front and top views of a nonnative SOD1 dimer observed in previous MD simulations of SOD1 misfolding (33). The residues 37–42 and 90–95 are colored in orange and blue, and pink and cyan, respectively, in the two monomers. Arrows indicate possible directions of fibril growth such that a cross-β structure results.

A Model for SOD1 Aggregation Based on the Destabilization of the β-Plug. Our results suggest that independent of the effect of mutation on the stability of the protein, FALS mutations alter the dynamics of SOD1 and weaken the network of hydrogen bonds stabilizing the β-plug residues providing evidence that local, as opposed to global, destabilization of SOD1 may be sufficient to induce aggregation. This destabilization of the β-plug upon exposure to three different aggregation-promoting conditions, combined with previous findings implicating the β-plug in SOD1 aggregation, suggests a model for the oligomerization of SOD1. We have previously identified the charged residues in the β5–β6 loop to be critical for the monomer folding and found that misfolded states result in computational studies of SOD1 folding when these interactions are disrupted (Fig. 4 *a* and *b*) (32). We have also previously observed in models of SOD1 aggregation that an opened SOD1 β-barrel has high propensity to swap strands with another similarly destabilized chain, particularly in the β5–β6 region (Fig. 4 *c* and *d*) (33). The enhanced destabilization of the β-plug region under three aggregation-promoting conditions reinforces a possible scenario of aggregation based on the opening of the SOD1 dimer. Locally destabilized SOD1 exposes the hydrogen bond donors and acceptors in the β5–β6 region and destabilizes the β-plug by the weakening of interactions of residues 90–95 with the residues 38–43 (Fig. 4*b*). Multiple open SOD1 monomers stack together at their opened exposed edges: the β-plug regions from neighboring monomers interact to form an alternative dimer, which may otherwise retain certain elements of the native structure (Fig. 4 *c* and *d*). The stacking together of such dimers may propagate the fibril (Fig. 4*d*). This mechanism is reminiscent of the "runaway domain-swapping" mechanism of aggregation proposed by Eisenberg and coworkers (34). Thus, our model suggests that, independent of FALS mutants stabilities, these mutants affect the dynamics of the β-plug, thereby promoting aggregation via domain swapping (33, 35).

While global destabilization of the native state is a widely accepted mechanism of protein aggregation, our results suggest that protein dynamics is also an important driving force underlying the aggregation of proteins. A structural understanding of SOD1

dynamics leading to its aggregation may aid the development of therapies for FALS aimed at the prevention of aggregation.

Materials and Methods

MD Simulations. We use the AMBER (36) MD simulation package to perform 5-ns-long MD simulations of monomers and dimers of the wild-type SOD (PDB entry 1SPD) at 300 and 400 K (for the wild-type dimer) and of three mutants A4V (PDB entry 1N19), G37R (PDB entry 1AZV), and H46R (PDB entry 1OZT). Because apo-SOD1 has been postulated to be implicated in disease, we remove metals from structures in which metals are present and use these as the starting structures for simulations. Starting with the atomic coordinates from the crystal structures, hydrogen atoms are added, and the protein is solvated in an octahedral box of TIP3P waters extending 10 Å from the protein. Counterions (Na^+) are added at appropriate places in the box to ensure charge-neutrality by using the LEAP module in AMBER. Periodic boundary conditions are applied throughout the simulation, and a nonbonded cutoff of 10 Å is used. Long-range electrostatic interactions are treated by particle mesh Ewald method as implemented in AMBER. The simulation protocol involves equilibration for 600 ps followed by a 5-ns production run at 300 or 400 K. The simulation protocol is described in detail in *Supporting Methods*, which is published as supporting information on the PNAS web site.

To compare the fluctuation of a given residue between various simulation trajectories after superimposition of the trajectory on the starting structure and removal of rotational and translational degrees of freedom, we calculate a Z score for the fluctuation value of the residue in the trajectory: $Z(i) = (f_i - \langle f_i \rangle)/\sigma$, where the fluctuation of a residue, i, is f_i, calculated from the PTRAJ module in AMBER, $\langle f_i \rangle$ is the average fluctuation of all residues in the protein, and σ is the standard deviation of the distribution of fluctuations. Thus, residues with a positive or negative value of $Z(i)$ fluctuate more or less than the average fluctuation of the protein, respectively. The $Z(i)$ values are related to the probability $\wp(Z) = 1/\sqrt{2\pi}\exp(-Z^2/2)$ of observing fluctuations f_i assuming, as a null-hypothesis, a Gaussian distribution of the fluctuation values f_i.

Covariance Matrices and Essential Dynamics Analysis. We calculate a C_α covariance matrix that describes the correlation of the positional shifts of C_α atoms in proteins:

$$c_{ij} = \langle (r_i - \langle r_i \rangle)(r_j - \langle r_j \rangle) \rangle, \qquad [1]$$

where r_i and r_j represent the coordinates of atoms i and j in a conformation, and $\langle \ldots \rangle$ represents the average over the trajectory. The average is calculated over all structures after they are superimposed on a reference (minimized crystal) structure to remove overall translational and rotational motion. To verify the robustness of the calculated correlation coefficients, we perform the covariance analysis over two nonoverlapping 2-ns-long subtrajectories corresponding to the last 4 ns of simulation time and find that the two matrices thus obtained are highly similar to the matrix obtained for the complete trajectory (data not shown). Diagonalizing the covariance matrix yields a set of eigenvectors and eigenvalues. The eigenvectors are directions in a $3N$-dimensional space (where N is the number of C_α atoms), and motion along a single eigenvector corresponds to concerted displacements of groups of atoms in the Cartesian "essential" subspace. The eigenvalues are a measure of the mean square fluctuation of the system along the corresponding eigenvectors.

Graph Theoretic Analysis. We represent the SOD1 structures as an undirected, unweighted graph $G = \{N_i, E_{ij}\}$, with nodes N_i corresponding to each residue i, and edges E_{ij} between the nodes N_i and N_j, if these are in contact. A contact between two residues exists if the distance between any pair of atoms (excluding hydrogen atoms) belonging to these residues is <4.2 Å (37). Two connected nodes are called neighbors of each other. A path between nodes N_i and N_j is defined as a set of edges that connect nodes N_i and N_j on G, the length of which is determined as the number of edges on the path. The minimal path is defined as the path of minimal length. We calculate for each residue (i) the average minimal path, L_i, between residue i and all other residues (38), and (ii) the betweenness, B_i, defined as the number of minimal paths passing through the given residue (39). For the residue-wise distributions of each of these properties, P_i, we obtain a Z score for each residue, which is a measure of the statistical significance: $Z(P_i) = (P_i - \langle P \rangle)/\sigma$, where P is any property, i.e., L or B, and $\langle P \rangle$ and σ are the average and standard deviation of the distribution $\{P_i\}$ correspondingly.

We thank F. Ding, Y. Chen, and B. Kuhlman for helpful discussions. This work was supported in part by Muscular Dystrophy Association Grant MDA3720 and March of Dimes Birth Defect Foundation Research Grant 5-FY03-155.

1. Valentine, J. S., Doucette, P. A. & Potter, S. Z. (2005) *Annu. Rev. Biochem.* **74,** 563–593.
2. Rosen, D. R., Siddique, T., Patterson, D., Figlewicz, D. A., Sapp, P., Hentati, A., Donaldson, D., Goto, J., Oregan, J. P., Deng, H. X., *et al.* (1993) *Nature* **362,** 59–62.
3. Gurney, M. E., Pu, H. F., Chiu, A. Y., Dalcanto, M. C., Polchow, C. Y., Alexander, D. D., Caliendo, J., Hentati, A., Kwon, Y. W., Deng, H. X., *et al.* (1994) *Science* **264,** 1772–1775.
4. Gaudette, M., Hirano, M. & Siddique, T. (2000) *Amyotrophic Lateral Scler. Other Motor Neuron Disorders* **1,** 83–89.
5. Cleveland, D. W. & Rothstein, J. D. (2001) *Nat. Rev. Neurosci.* **2,** 806–819.
6. Okado-Matsumoto, A. & Fridovich, I. (2002) *Proc. Natl. Acad. Sci. USA* **99,** 9010–9014.
7. Bruening, W., Roy, J., Giasson, B., Figlewicz, D. A., Mushynski, W. E. & Durham, H. D. (1999) *J. Neurochem.* **72,** 693–699.
8. Khare, S. D., Caplow, M. & Dokholyan, N. V. (2004) *Proc. Natl. Acad. Sci. USA* **101,** 15094–15099.
9. Ray, S. S., Nowak, R. J., Strokovich, K., Brown, R. H., Walz, T. & Lansbury, P. T. (2004) *Biochemistry* **43,** 4899–4905.
10. Rakhit, R., Crow, J. P., Lepock, J. R., Kondejewski, L. H., Cashman, N. R. & Chakrabartty, A. (2004) *J. Biol. Chem.* **279,** 15499–15504.
11. Ray, S. S., Nowak, R. J., Brown, R. H. & Lansbury, P. T. (2005) *Proc. Natl. Acad. Sci. USA* **102,** 3639–3644.
12. Lindberg, M. J., Tibell, L. & Oliveberg, M. (2002) *Proc. Natl. Acad. Sci. USA* **99,** 16607–16612.
13. Lindberg, M. J., Bystrom, R., Boknas, N., Andersen, P. M. & Oliveberg, M. (2005) *Proc. Natl. Acad. Sci. USA* **102,** 9754–9759.
14. Rodriguez, J. A., Shaw, B. F., Durazo, A., Sohn, S. H., Doucette, P. A., Nersissian, A. M., Faull, K. F., Eggers, D. K., Tiwari, A., Hayward, L. J., *et al.* (2005) *Proc. Natl. Acad. Sci. USA* **102,** 10516–10521.
15. Tiwari, A. & Hayward, L. J. (2003) *J. Biol. Chem.* **278,** 5984–5992.
16. Tiwari, A., Xu, Z. S. & Hayward, L. J. (2005) *J. Biol. Chem.* **280,** 29771–29779.
17. Shipp, E. L., Cantini, F., Bertini, I., Valentine, J. S. & Banci, L. (2003) *Biochemistry* **42,** 1890–1899.
18. Lockless, S. W. & Ranganathan, R. (1999) *Science* **286,** 295–299.
19. Suel, G. M., Lockless, S. W., Wall, M. A. & Ranganathan, R. (2003) *Nat. Struct. Biol.* **10,** 59–69.
20. Fuentes, E. J., Der, C. J. & Lee, A. L. (2004) *J. Mol. Biol.* **335,** 1105–1115.
21. Gunasekaran, K., Nussinov, R. & Ma, B. (2004) *Proteins Struct. Funct. Bioinformat.* **57,** 433–443.
22. Hart, P. J., Liu, H. B., Pellegrini, M., Nersissian, A. M., Gralla, E. B., Valentine, J. S. & Eisenberg, D. (1998) *Protein Sci.* **7,** 545–555.
23. Chillemi, G., Falconi, M., Amadei, A., Zimatore, G., Desideri, A. & DiNola, A. (1997) *Biophys. J.* **73,** 1007–1018.
24. Luo, J. & Bruice, T. C. (2004) *Proc. Natl. Acad. Sci. USA* **101,** 13152–13156.
25. Amadei, A., Linssen, A. B. M. & Berendsen, H. J. C. (1993) *Proteins Struct. Funct. Bioinformat.* **17,** 412–425.
26. Silva, N. D., Gratton, E., Mei, G., Rosato, N. & FinazziAgro, A. (1992) *FASEB J.* **6,** A311.
27. Ferraroni, M., Rypniewski, W., Wilson, K. S., Viezzoli, M. S., Banci, L., Bertini, I. & Mangani, S. (1999) *J. Mol. Biol.* **288,** 413–426.
28. Banci, L., Bertini, I., Cramaro, F., Del Conte, R., Rosato, A. & Viezzoli, M. S. (2000) *Biochemistry* **39,** 9108–9118.
29. Strange, R. W., Antonyuk, S., Hough, M. A., Doucette, P. A., Rodriguez, J. A., Hart, P. J., Hayward, L. J., Valentine, J. S. & Hasnain, S. S. (2003) *J. Mol. Biol.* **328,** 877–891.
30. Elam, J. S., Taylor, A. B., Strange, R., Antonyuk, S., Doucette, P. A., Rodriguez, J. A., Hasnain, S. S., Hayward, L. J., Valentine, J. S., Yeates, T. O., *et al.* (2003) *Nat. Struct. Biol.* **10,** 461–467.
31. Richardson, J. S. & Richardson, D. C. (2002) *Proc. Natl. Acad. Sci. USA* **99,** 2754–2759.
32. Khare, S. D., Ding, F. & Dokholyan, N. V. (2003) *J. Mol. Biol.* **334,** 515–525.
33. Khare, S. D., Wilcox, K. C., Gong, P. & Dokholyan, N. V. (2005) *Proteins Struct. Funct. Bioinformat.* **61,** 617–632.
34. Sambashivan, S., Liu, Y. S., Sawaya, M. R., Gingery, M. & Eisenberg, D. (2005) *Nature* **437,** 266–269.
35. Ding, F., Prutzman, K. C., Campbell, S. L. & Dokholyan, N. V. (2006) *Structure* **14,** 5–14.
36. Pearlman, D. A., Case, D. A., Caldwell, J. W., Ross, W. S., Cheatham, T. E., Debolt, S. E., Ferguson, D. M., Seibel, G. L. & Kollman, P. A. (1995) *Comput. Phys. Commun.* **91,** 1–41.
37. Mirny, L. & Domany, E. (1996) *Proteins Struct. Funct. Genet.* **26,** 391–410.
38. Dokholyan, N. V., Li, L., Ding, F. & Shakhnovich, E. I. (2002) *Proc. Natl. Acad. Sci. USA* **99,** 8637–8641.
39. Dokholyan, N. V. (2005) *Gene* **347,** 199–206.